https://doi.org/10.1038/s41586-019-1496-5

Superconductivity in an infinite-layer nickelate

Danfeng Li[1,2]*, Kyuho Lee[1,3], Bai Yang Wang[1,3], Motoki Osada[1,4], Samuel Crossley[1,2], Hye Ryoung Lee[1,4], Yi Cui[1,4], Yasuyuki Hikita[1] & Harold Y. Hwang[1,2]*

The discovery of unconventional superconductivity in $(La,Ba)_2CuO_4$ (ref. [1]) has motivated the study of compounds with similar crystal and electronic structure, with the aim of finding additional superconductors and understanding the origins of copper oxide superconductivity. Isostructural examples include bulk superconducting Sr_2RuO_4 (ref. [2]) and surface-electron-doped Sr_2IrO_4, which exhibits spectroscopic signatures consistent with a superconducting gap[3,4], although a zero-resistance state has not yet been observed. This approach has also led to the theoretical investigation of nickelates[5,6], as well as thin-film heterostructures designed to host superconductivity. One such structure is the $LaAlO_3/LaNiO_3$ superlattice[7–9], which has been recently proposed for the creation of an artificially layered nickelate heterostructure with a singly occupied $d_{x^2-y^2}$ band. The absence of superconductivity observed in previous related experiments has been attributed, at least in part, to incomplete polarization of the e_g orbitals[10]. Here we report the observation of superconductivity in an infinite-layer nickelate that is isostructural to infinite-layer copper oxides[11–13]. Using soft-chemistry topotactic reduction[14–20], $NdNiO_2$ and $Nd_{0.8}Sr_{0.2}NiO_2$ single-crystal thin films are synthesized by reducing the perovskite precursor phase. Whereas $NdNiO_2$ exhibits a resistive upturn at low temperature, measurements of the resistivity, critical current density and magnetic-field response of $Nd_{0.8}Sr_{0.2}NiO_2$ indicate a superconducting transition temperature of about 9 to 15 kelvin. Because this compound is a member of a series of reduced layered nickelate crystal structures[21–23], these results suggest the possibility of a family of nickelate superconductors analogous to copper oxides[24] and pnictides[25].

The most stable nickelates have a formal valence of Ni^{2+} and a d^8 electronic configuration, such as in NiO and La_2NiO_4, but they can also form with d^7 Ni^{3+}, as in $LaNiO_3$. Mimicking the d^9 configuration of undoped copper oxides requires the highly unusual valence Ni^{+}. Although this oxidation state cannot be reached by conventional high-temperature synthesis, it was found that low-temperature reduction of $LaNiO_3$ can induce a topochemical reaction to form $LaNiO_2$[14,15]. (In general, slight oxygen off-stoichiometry is possible, but for simplicity we use the stoichiometric formula throughout this manuscript.) Subsequently, it was shown that this oxygen deintercalation also occurs in epitaxial thin films, with the useful feature that the substrate can provide a template that preserves single-crystal *c*-axis-oriented $LaNiO_2$ (Fig. 1) in the vicinity of the substrate[17–19]. In this structure, nickel has square planar oxygen coordination in two-dimensional NiO_2 planes (alternating with planes of La), with a predicted d^9 configuration leaving one hole in the $d_{x^2-y^2}$ orbital and therefore a possible distinct orbital polarization[5]. Indeed such large preferential orbital occupancy near the Fermi level has been observed in the related trilayer reduced nickelate $La_4Ni_3O_8$ (nominally $Ni^{1.33+}$, $d^{8.67}$)[23].

In preliminary work, we first synthesized $LaNiO_3$ thin films on single-crystal $SrTiO_3$ (001) substrates by pulsed-laser deposition, followed by a reduction step using CaH_2 powder as a reagent (see Methods). Whereas $LaNiO_3$ was metallic down to low temperatures, $LaNiO_2$ was weakly insulating, consistent with previous reports[17,18]. Given that perovskite nickelates can be doped by chemical substitution on the rare-earth site[26,27], we then explored reduced $La_{1-x}Sr_xNiO_2$ thin films as an approach to hole-dope the parent compound. Although the conductivity was enhanced (maximally for $x \approx 0.2$; data not shown), in all cases the resistivity exhibited insulating temperature dependence below about 150 K. Although this result should not be considered definitive (it may depend on further optimization of the growth conditions and reduction process), we then turned to $NdNiO_2$ in an attempt to increase the electronic bandwidth via the smaller ionic radius of Nd with respect to La, which results in a smaller cell volume[15,16]. This tendency has been observed in trilayer reduced nickelates, where $La_4Ni_3O_8$ is insulating, whereas $Pr_4Ni_3O_8$ is metallic down to low temperature[23]. With these motivations, we focused our efforts on optimizing and investigating $NdNiO_2$ and $Nd_{0.8}Sr_{0.2}NiO_2$, which we present in detail here.

Bulk $NdNiO_3$ is orthorhombic with room-temperature lattice parameters $a = 5.39$ Å, $b = 5.38$ Å and $c = 7.61$ Å (a pseudocubic lattice parameter of about 3.81 Å), and doping with Sr has no substantial influence on its room-temperature structure and lattice constants[27]. $NdNiO_2$ reduced from $NdNiO_3$ has been previously synthesized in both polycrystalline[16] and thin-film form[20], and was reasonably straightforward to grow. By contrast, we found that the synthesis of thin-film $Nd_{0.8}Sr_{0.2}NiO_3$ is more challenging—presumably because of the high Ni oxidation state and reduced tolerance factor compared to $LaNiO_3$ (ref. [28]). Figure 2a shows an X-ray diffraction (XRD) θ–2θ symmetric scan of a $Nd_{0.8}Sr_{0.2}NiO_3$ film grown under conditions optimized using XRD, revealing only clear (001) and (002) perovskite peaks (see Methods; 2θ, diffraction angle). (Throughout much of this work we used a $SrTiO_3$ epitaxial capping layer to protect the reduced nickelate films from potential degradation, unless otherwise noted.) From their positions, the *c*-axis lattice constant was extracted to be 3.77 Å, in line with a film under epitaxial tensile strain imposed by the $SrTiO_3$ substrate. Figure 2a also shows the θ–2θ diffraction pattern of the film after reduction, showing peaks with 2θ values of 26.3° and 54.3° corresponding to the (001) and (002) peaks of the infinite-layer phase, respectively, confirming the transformation to $Nd_{0.8}Sr_{0.2}NiO_2$ (refs [16,17]). In measurements with diffraction angles up to $2\theta = 114°$ (not shown) the (003) film peak is not visible owing to its low intensity, whereas the (004) peak falls beyond the diffractometer limit, and no other peaks are observed. Both before and after reduction, the film was always clamped to the in-plane $SrTiO_3$ lattice (Fig. 2b, c).

In bulk undoped $NdNiO_3$, reducing the perovskite to the infinite-layer phase (reported for $NdNiO_{2.03}$) leads to an expansion of the in-plane lattice constants (about 3.92 Å), along with a shortened *c* axis (about 3.31 Å)[16], which is the distance between adjacent Ni–O planes. From the (00*l*) peak positions of the $Nd_{0.8}Sr_{0.2}NiO_2$ film, the *c*-axis lattice constant is found to be 3.37 Å, and it ranges from 3.34 Å to 3.38 Å in samples prepared in nominally similar conditions. The film experiences compressive strain on the $SrTiO_3$ (3.91 Å) substrate, as well as potential *c*-axis expansion due to the partial substitution of Nd by the larger Sr ion. We note, however, that the metallic nature of $Nd_{0.8}Sr_{0.2}NiO_2$ counteracts these trends. No signature of a fluorite defect phase[20] was observed in asymmetric θ–2θ XRD scans of our samples (both doped

[1]Stanford Institute for Materials and Energy Sciences, SLAC National Accelerator Laboratory, Menlo Park, CA, USA. [2]Department of Applied Physics, Stanford University, Stanford, CA, USA. [3]Department of Physics, Stanford University, Stanford, CA, USA. [4]Department of Materials Science and Engineering, Stanford University, Stanford, CA, USA. *e-mail: denverli@stanford.edu; hyhwang@stanford.edu

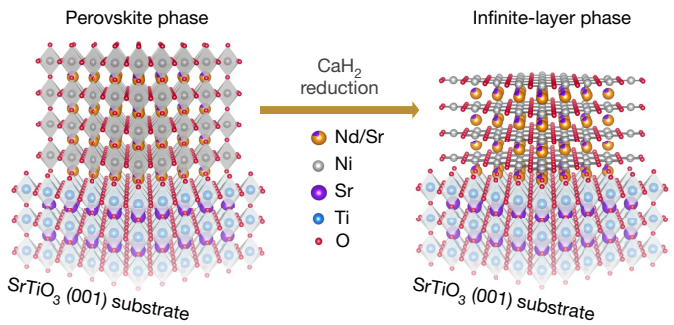

Fig. 1 | Topotactic reduction of nickelate thin films. Schematic crystal structures of $Nd_{0.8}Sr_{0.2}NiO_3$ (left) and $Nd_{0.8}Sr_{0.2}NiO_2$ (right) thin films on the TiO_2-terminated single-crystal $SrTiO_3$ (001) substrate. Upon low-temperature reduction, the films undergo a topotactic transition from the perovskite phase to the infinite-layer phase.

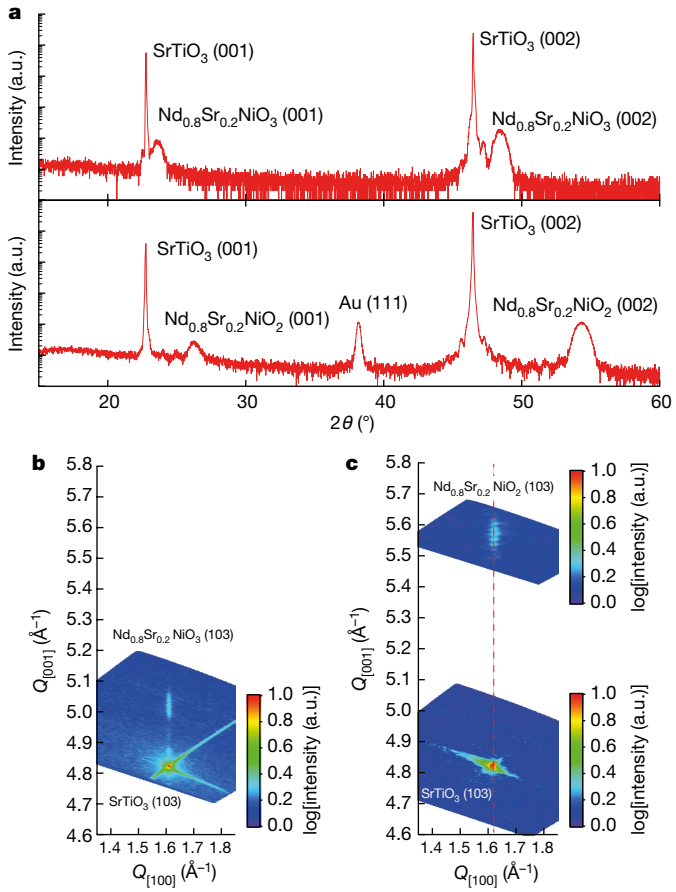

Fig. 2 | Structural characterization of the doped nickelate thin films. **a**, X-ray diffraction θ–2θ symmetric scans of 11-nm-thick $Nd_{0.8}Sr_{0.2}NiO_3$ (top) and $Nd_{0.8}Sr_{0.2}NiO_2$ (bottom; with contribution from gold contacts) films capped with 20-nm-thick $SrTiO_3$ layers grown on $SrTiO_3$ (001) substrates. **b, c**, Reciprocal space maps of $Nd_{0.8}Sr_{0.2}NiO_3$ (**b**) and $Nd_{0.8}Sr_{0.2}NiO_2$ (**c**) around the (103) $SrTiO_3$ diffraction peak. Both maps indicate that the films are fully strained to the $SrTiO_3$ substrates. a.u., arbitrary units.

and undoped). For thin-film $LaNiO_3$, reduction induces a series of transformation steps: first to brownmillerite $LaNiO_{2.5}$, then to *c*-axis $LaNiO_2$, followed by a reorientation transition to *a*-axis $LaNiO_2$, before subsequent decomposition[29]. For $NdNiO_3$ and $Nd_{0.8}Sr_{0.2}NiO_3$, we only observe a direct transition to the *c*-axis infinite-layer structure (Fig. 1). Our annealing conditions (see Methods) are empirically optimized to maximize the XRD infinite-layer peak intensity and minimize the *c*-axis lattice constant (as a proxy for the removal of apical oxygen). The comparable (002) peak intensities for the perovskite and infinite-layer phases (Fig. 2a), as well as the thickness fringes observed near (002) after reduction, indicate a complete structural transformation of the film. Reduction for much longer times or at higher temperature induces decomposition of the film, and no XRD features are observed.

Figure 3a shows the temperature-dependent resistivity $\rho(T)$ of $NdNiO_3$ and $Nd_{0.8}Sr_{0.2}NiO_3$. $NdNiO_3$ shows the characteristic first-order phase transition from a high-temperature paramagnetic metal to a low-temperature charge-disproportionated antiferromagnetic insulator, which is suppressed with Sr doping[26,27]. After reduction (Fig. 3b), we find that $NdNiO_2$ displays metallic temperature dependence at high temperatures, with a resistive upturn below about 70 K. By contrast, $Nd_{0.8}Sr_{0.2}NiO_2$ exhibits metallic behaviour followed by a superconducting transition, with an onset at 14.9 K (point of maximum curvature), a midpoint at 13.6 K and zero resistance at 9.1 K (indistinguishable from the noise floor) for this sample. The temperature-dependent normal-state Hall coefficient $R_H(T)$ is given in Fig. 3c. R_H for $NdNiO_2$ is negative at all temperatures, whereas it undergoes a sign change at about 55 K for $Nd_{0.8}Sr_{0.2}NiO_2$. This feature, as well as the overall magnitude of R_H, are inconsistent with the expectations for simple hole doping of a single electronic band, and suggest a more complex Fermi surface. This may be consistent with calculations of the electronic band structure of $LaNiO_2$, which find multiple electron and hole pockets that have different orbital contributions[6] and that vary with the Coulomb interaction. We further note that the interface between the infinite-layer nickelate and the $SrTiO_3$ substrate (Fig. 1) hosts a strong polar discontinuity[30]. Depending on how this electrostatic boundary condition is resolved, there may be transport contributions from interface states. However, the comparison between $NdNiO_2$ and $Nd_{0.8}Sr_{0.2}NiO_2$ demonstrates that this alone does not lead to superconductivity here.

The observation of superconductivity is quite robust. In Fig. 3d, e we show a number of different samples of $Nd_{0.8}Sr_{0.2}NiO_2$ synthesized in nominally similar conditions. The origin of the variation in transition temperature (T_c) is unclear, but there are some indications that it correlates with the crystallinity of the parent perovskite phase and may also reflect slight variations in the oxygen stoichiometry. In Figs. 3f, 4 we focus on one sample (Fig. 3b) with a high transition temperature; all other samples showed similar behaviour as scaled by T_c. Figure 3f shows measurements of the temperature-dependent current–voltage characteristics for this sample. These features are linear in the normal state (outside nonlinearities due to Joule heating at high bias) and increasingly nonlinear below the transition, and they are characteristic of superconductivity with a critical current density $J_c(2\ \mathrm{K}) \approx 170\ \mathrm{kA\ cm^{-2}}$.

Figure 4a displays the temperature-dependent magnetoresistance measured in magnetic fields perpendicular to the plane of the sample, up to 13 T. The normal state exhibits very little magnetoresistance, whereas superconductivity is suppressed with increasing field. As a proxy for the variation of the upper critical field $H_{c,\perp}$, we take the midpoint of the resistive transition to the normal state near T_c and fit it to the linearized Ginzburg–Landau form

$$H_{c,\perp}(T) = \frac{\Phi_0}{2\pi\xi_{GL}^2(0)}\left(1 - \frac{T}{T_c}\right)$$

where Φ_0 is the flux quantum and $\xi_{GL}(0)$ is the extrapolated zero-temperature Ginzburg–Landau coherence length, which we find to be 3.25 ± 0.01 nm. (This estimate does not consider potential contributions from vortex motion or variations due to sample inhomogeneity.) We further perform two-coil mutual-inductance measurements in the perpendicular geometry, as shown in Fig. 4b. Here we plot the real ($\mathrm{Re}(V_p)$) and imaginary ($\mathrm{Im}(V_p)$) components of the a.c. voltage signal detected by the pickup coil above the sample. As the sample is cooled through the transition, $\mathrm{Re}(V_p)$ decreases while $\mathrm{Im}(V_p)$ exhibits a peak, indicating an emergent diamagnetic response below the transition as the magnetic field generated from the drive coil becomes screened by the superconductor. The fact that $\mathrm{Re}(V_p)$ does not approach zero at low

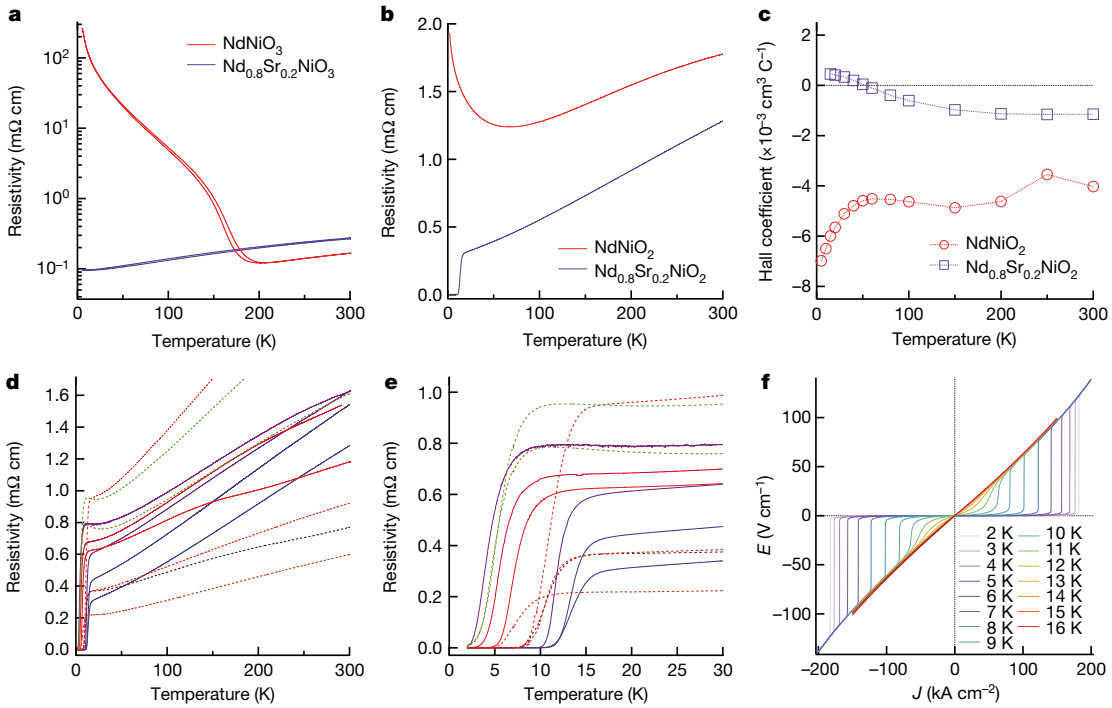

Fig. 3 | Transport properties and superconductivity of the nickelate thin films. a, Resistivity versus temperature $\rho(T)$ plots of the as-grown $NdNiO_3$ and $Nd_{0.8}Sr_{0.2}NiO_3$ films. **b, c**, Resistivity (**b**) and normal-state Hall coefficient (**c**) as a function of temperature for the corresponding reduced films ($NdNiO_2$ and $Nd_{0.8}Sr_{0.2}NiO_2$). **d, e**, $\rho(T)$ for multiple $Nd_{0.8}Sr_{0.2}NiO_2$ films, showing resistive superconducting transitions. Dotted lines indicate samples without a capping layer, for which the XRD Scherrer thickness was used to estimate the resistivity. **f**, Electric field (E) versus current density (J) characteristics for varying temperature.

temperatures resembles measurement results of a 40-nm-thick infinite-layer copper oxide film with $T_c \approx 10.8$ K and extrapolated London penetration depth $\lambda_L(T=0) = 2.2\ \mu m$ (ref. [31]). This indicates that λ_L for $Nd_{0.8}Sr_{0.2}NiO_2$ is similarly large compared to the film thickness. Given the numerical uncertainties arising from the finite sample size (substantially wider films show indications of laterally inhomogeneous reduction), the order parameter symmetry and the scale of disorder, we did not attempt to extract λ_L (ref. [32]). Nevertheless, these data suggest that this is a type-II superconductor with second critical field $H_{c2,\perp}$ approximately given in the inset to Fig. 4a.

Clearly the analogy to copper oxides motivated this finding, and much remains to be explored in this new superconducting compound. However, several important dissimilarities between these two systems are apparent. One key difference is the energy level alignments in their orbital electronic structure. Holes in copper oxides are often discussed in terms of Zhang–Rice singlets with strong oxygen character, owing to the close spatial overlap and near-energetic degeneracy of the Cu $d_{x^2-y^2}$ orbitals and the O $2p$ orbitals[33]. This naturally leads to large in-plane antiferromagnetic coupling, which many consider to be central for superconducting pairing[24]. Because Ni^+ is one column to the left of Cu^{2+} on the periodic table and one oxidation state lower, the chemical potential in the infinite-layer nickelates is several electronvolts higher than that of comparable copper oxides; therefore, in hole-doped nickelates, much less hybridization with the O $2p$ band is expected[6]. Furthermore, powder neutron diffraction studies of $LaNiO_2$ and $NdNiO_2$ show no indication of magnetic order down to 5 K and 1.7 K, respectively[15,16], and the resistivity of $NdNiO_2$ (Fig. 3b) is inconsistent with a robust insulator (although interface effects may contribute to conductivity). Consequently, two features that are central to copper oxides—the Zhang–Rice singlet and large planar spin fluctuations—may be absent (or considerably diminished) in these nickelate superconductors.

On the materials side, one immediate question is the effect of the various substrates on the topotactic structural transition of this

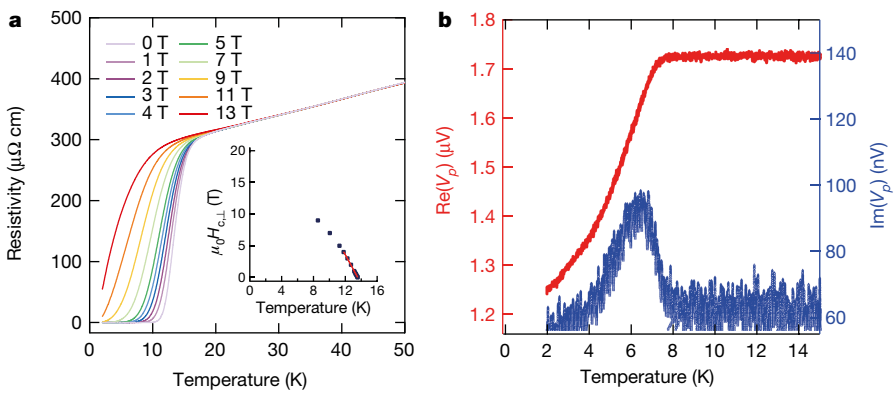

Fig. 4 | Magnetic-field response of superconducting $Nd_{0.8}Sr_{0.2}NiO_2$. a, $\rho(T)$ under a varying magnetic field perpendicular to the a–b plane. The inset shows the variation of the upper critical field $H_{c,\perp}$ (as estimated by the midpoint of the resistive transition) with a linear fit in the vicinity of T_c. **b**, The real ($\mathrm{Re}(V_p)$) and imaginary ($\mathrm{Im}(V_p)$) parts of the voltage as a function of temperature in the pickup coil on a $Nd_{0.8}Sr_{0.2}NiO_2$ film, measured using a two-coil mutual-inductance measurement. μ_0, magnetic constant.

system and the associated dependence of superconductivity on epitaxial strain. Here we have an unusual situation in which the substrate that stabilizes the phase also strains it. Another important question is whether there is a doping-dependent superconducting dome, as found in copper oxides[24]. We believe that our approach to chemical substitution is broadly applicable and can address this issue, but the central challenge will be whether complex reduction chemistry can be homogeneously controlled across a range of unconventional nickel oxidation states.

Online content

Any methods, additional references, Nature Research reporting summaries, source data, extended data, supplementary information, acknowledgements, peer review information; details of author contributions and competing interests; and statements of data and code availability are available at https://doi.org/10.1038/s41586-019-1496-5.

Received: 29 June 2019; Accepted: 30 July 2019;
Published online 28 August 2019.

1. Bednorz, J. G. & Müller, K. A. Possible high T_c superconductivity in the Ba-La-Cu-O system. *Z. Phys. B* **64**, 189–193 (1986).
2. Maeno, Y. et al. Superconductivity in a layered perovskite without copper. *Nature* **372**, 532–534 (1994).
3. Yan, Y. J. et al. Electron-doped Sr_2IrO_4: an analogue of hole-doped cuprate superconductors demonstrated by scanning tunneling microscopy. *Phys. Rev. X* **5**, 041018 (2015).
4. Kim, Y. K., Sung, N. H., Denlinger, J. D. & Kim, B. J. Observation of a *d*-wave gap in electron-doped Sr_2IrO_4. *Nat. Phys.* **12**, 37–41 (2016).
5. Anisimov, V. I., Bukhvalov, D. & Rice, T. M. Electronic structure of possible nickelate analogs to the cuprates. *Phys. Rev. B* **59**, 7901–7906 (1999).
6. Lee, K.-W. & Pickett, W. E. Infinite-layer $LaNiO_2$: Ni^{1+} is not Cu^{2+}. *Phys. Rev. B* **70**, 165109 (2004).
7. Chaloupka, J. & Khaliullin, G. Orbital order and possible superconductivity in $LaNiO_3/LaMO_3$ superlattices. *Phys. Rev. Lett.* **100**, 016404 (2008).
8. Hansmann, P. et al. Turning a nickelate Fermi surface into a cuprate-like one through heterostructuring. *Phys. Rev. Lett.* **103**, 016401 (2009).
9. Han, M. J., Wang, X., Marianetti, C. A. & Millis, A. J. Dynamical mean-field theory of nickelate superlattices. *Phys. Rev. Lett.* **107**, 206804 (2011); erratum **110**, 179904 (2013).
10. Disa, A. S. et al. Orbital engineering in symmetry-breaking polar heterostructures. *Phys. Rev. Lett.* **114**, 026801 (2015).
11. Siegrist, T., Zahurak, S. M., Murphy, D. W. & Roth, R. S. The parent structure of the layered high-temperature superconductors. *Nature* **334**, 231–232 (1988).
12. Smith, M. G., Manthiram, A., Zhou, J., Goodenough, J. B. & Markert, J. T. Electron-doped superconductivity at 40 K in the infinite-layer compound $Sr_{1-y}Nd_yCuO_2$. *Nature* **351**, 549–551 (1991).
13. Azuma, M., Hiroi, Z., Takano, M., Bando, Y. & Takeda, Y. Superconductivity at 110 K in the infinite-layer compound $(Sr_{1-x}Ca_x)_{1-y}CuO_2$. *Nature* **356**, 775–776 (1992).
14. Crespin, M., Levitz, P. & Gatineau, L. Reduced forms of $LaNiO_3$ perovskite. Part 1.—Evidence for new phases: $La_2Ni_2O_5$ and $LaNiO_2$. *J. Chem. Soc. Faraday Trans. II* **79**, 1181–1194 (1983).
15. Hayward, M. A., Green, M. A., Rosseinsky, M. J. & Sloan, J. Sodium hydride as a powerful reducing agent for topotactic oxide deintercalation: synthesis and characterization of the nickel(I) oxide $LaNiO_2$. *J. Am. Chem. Soc.* **121**, 8843–8854 (1999).
16. Hayward, M. A. & Rosseinsky, M. J. Synthesis of the infinite layer Ni(I) phase $NdNiO_{2+x}$ by low temperature reduction of $NdNiO_3$ with sodium hydride. *Solid State Sci.* **5**, 839–850 (2003).
17. Kawai, M. et al. Reversible changes of epitaxial thin films from perovskite $LaNiO_3$ to infinite-layer structure $LaNiO_2$. *Appl. Phys. Lett.* **94**, 082102 (2009).
18. Kaneko, D., Yamagishi, K., Tsukada, A., Manabe, T. & Naito, M. Synthesis of infinite-layer $LaNiO_2$ films by metal organic decomposition. *Physica C* **469**, 936–939 (2009).
19. Ikeda, A., Krockenberger, Y., Irie, H., Naito, M. & Yamamoto, H. Direct observation of infinite NiO_2 planes in $LaNiO_2$ films. *Appl. Phys. Express* **9**, 061101 (2016).
20. Onozuka, T., Chikamatsu, A., Katayama, T., Fukumura, T. & Hasegawa, T. Formation of defect-fluorite structured $NdNiO_xH_y$ epitaxial thin films via a soft chemical route from $NdNiO_3$ precursors. *Dalton Trans.* **45**, 12114–12118 (2016).
21. Lacorre, P. Passage from T-type to T′-type arrangement by reducing $R_4Ni_3O_{10}$ to $R_4Ni_3O_8$ (R = La, Pr, Nd). *J. Solid State Chem.* **97**, 495–500 (1992).
22. Poltavets, V. V. et al. $La_3Ni_2O_6$: a new double T′-type nickelate with infinite $Ni^{1+/2+}O_2$ layers. *J. Am. Chem. Soc.* **128**, 9050–9051 (2006).
23. Zhang, J. et al. Large orbital polarization in a metallic square-planar nickelate. *Nat. Phys.* **13**, 864–869 (2017).
24. Keimer, B., Kivelson, S. A., Norman, M. R., Uchida, S. & Zaanen, J. From quantum matter to high-temperature superconductivity in copper oxides. *Nature* **518**, 179–186 (2015).
25. Hosono, H. & Kuroki, K. Iron-based superconductors: current status of materials and pairing mechanism. *Physica C* **514**, 399–422 (2015).
26. Cheong, S.-W., Hwang, H. Y., Batlogg, B., Cooper, A. S. & Canfield, P. C. Electron-hole doping of the metal-insulator transition compound $RENiO_3$. *Physica B* **194–196**, 1087–1088 (1994).
27. García-Muñoz, J. L., Suaaidi, M., Martínez-Lope, M. J. & Alonso, J. A. Influence of carrier injection on the metal-insulator transition in electron- and hole-doped $R_{1-x}A_xNiO_3$ perovskite. *Phys. Rev. B* **52**, 13563–13569 (1995).
28. Torrance, J. B., Lacorre, P., Nazzal, A. I., Ansaldo, E. J. & Niedermayer, C. Systematic study of insulator-metal transitions in perovskites $RNiO_3$ (R=Pr, Nd, Sm, Eu) due to closing of charge-transfer gap. *Phys. Rev. B* **45**, 8209–8212 (1992).
29. Kawai, M. et al. Orientation change of an infinite-layer structure $LaNiO_2$ epitaxial thin film by annealing with CaH_2. *Cryst. Growth Des.* **10**, 2044–2046 (2010).
30. Nakagawa, N., Hwang, H. Y. & Muller, D. A. Why some interfaces cannot be sharp. *Nat. Mater.* **5**, 204–209 (2006).
31. Fruchter, L. et al. Penetration depth of electron-doped infinite-layer $Sr_{0.88}La_{0.12}CuO_{2+x}$ thin films. *Phys. Rev. B* **82**, 144529 (2010).
32. He, X., Gozar, A., Sundling, R. & Božović, I. High-precision measurement of magnetic penetration depth in superconducting films. *Rev. Sci. Instrum.* **87**, 113903 (2016).
33. Zhang, F. C. & Rice, T. M. Effective Hamiltonian for the superconducting Cu oxides. *Phys. Rev. B* **37**, 3759–3761 (1988).

METHODS

Film growth. TiO_2-terminated $SrTiO_3$ (001) substrates of size 5×5 mm^2 were pre-annealed at an oxygen partial pressure $P_{O2} = 5 \times 10^{-6}$ torr for 30 min at 950 °C to achieve sharp step-and-terrace surfaces. 9–11-nm-thick perovskite $NdNiO_3$ and $Nd_{0.8}Sr_{0.2}NiO_3$ films were grown on the annealed substrates by pulsed-laser deposition using a 248-nm KrF excimer laser. This thickness was chosen because it was approximately equal to the maximum thickness for which we could verify the formation of a uniform, single-phase infinite-layer film after reduction using XRD. $NdNiO_3$ ($Nd_{0.8}Sr_{0.2}NiO_3$) films were deposited at a substrate temperature of $T_g = 600$ °C and $P_{O2} = 150$ mtorr, using a laser fluence of 2 J cm^{-2} on the target. Subsequently, $SrTiO_3$ epitaxial capping layers (typically 20 nm thick) were deposited at $T_g = 570$ °C and the same P_{O2}, using a laser fluence of 0.8 J cm^{-2}. After growth, the samples were cooled to room temperature in the same oxygen environment. The nickelate targets were prepared by sintering mixtures of stoichiometric amounts of Nd_2O_3, $SrCO_3$ and NiO powder at 1,350 °C for 12 h, with two intermediate grinding and pelletizing steps after the initial decarbonation step at 1,200 °C for 12 h.

Reduction process. After growth, each sample was cut into two pieces of size 2.5×5 mm^2. Each piece (loosely wrapped in aluminium foil) was then vacuum-sealed together with about 0.1 g of CaH_2 powder in a Pyrex glass tube (pressure <0.1 mtorr). In this way, the pieces were not in direct contact with the CaH_2 powder[14–18], but underwent a gas-phase reaction with the powder upon annealing. The tube was heated to 260–280 °C at a rate of 10 °C min^{-1} and kept at this temperature for 4–6 h; then it was cooled to room temperature at a rate of 10 °C min^{-1}.

Characterization. The XRD data were taken using a monochromated Cu Kα_1 source. The resistivity, magnetotransport and current–voltage characteristic measurements were conducted in a six-point geometry using Au and Al wire-bonded contacts. In some cases, Au contact pads were first deposited using electron-beam evaporation. Critical-current density–voltage measurements were performed on a narrow channel defined by a diamond scribe, approximately 0.2 mm wide.

Mutual-inductance measurements. The $Nd_{0.8}Sr_{0.2}NiO_2$ samples were placed tightly between two collinear coils, the mutual inductance of which was sensitive to diamagnetic screening of the sample in the superconducting phase. The twin 80-turn coils had inner diameter of about 0.5 mm and outer diameter of around 1.5 mm, yielding a measured self-inductance of about 6 μH. The drive coil was driven with an alternating current of root-mean-square amplitude of 100 μA and frequency of 15 kHz. The in-phase and out-of-phase components of the voltage across the pickup coil (in the microvolt and submicrovolt range, respectively) were measured by lock-in amplification. The measured voltage was in a regime of linear response with respect to the amplitude of the drive current.

Data availability

The data presented in the figures and other findings of this study are available from the corresponding authors upon reasonable request.

Acknowledgements We thank A. Kapitulnik, S. A. Kivelson, W.-S. Lee, Y. Z. Li, S. Raghu and Z. X. Shen for discussions. This work was supported by the US Department of Energy, Office of Basic Energy Sciences, Division of Materials Sciences and Engineering, under contract number DE-AC02-76SF00515. D.L. acknowledges partial support by the Swiss National Science Foundation, and the Gordon and Betty Moore Foundation's Emergent Phenomena in Quantum Systems Initiative through grant number GBMF4415, which also supported S.C. and provided synthesis equipment. M.O. acknowledges partial financial support from the Takenaka Scholarship Foundation.

Author contributions D.L., Y.H. and H.Y.H. conceived the project. D.L. and M.O. grew the nickelate films and conducted the reduction experiments. K.L., D.L., M.O., H.R.L. and Y.C. conducted materials and structural characterization. B.Y.W., S.C. and D.L. performed the transport and mutual-inductance measurements. D.L. and H.Y.H. wrote the manuscript with contribution from all authors.

Competing interests The authors declare no competing interests.

Additional information

Correspondence and requests for materials should be addressed to D.L. or H.Y.H.

Peer review information *Nature* thanks George Sawatzky and the other, anonymous, reviewer(s) for their contribution to the peer review of this work.